

Styryl-cyanine dyes: State of the art and applications in bioimaging

Kotchakorn Supabowornsathit^{a,b}, Kriangsak Faikhruea^{a,b}, Tirayut Vilaivan^{a,*,†}

^a Organic Synthesis Research Unit, Department of Chemistry, Faculty of Science, Chulalongkorn University, Bangkok 10330 Thailand

^b Synna Science Co., Ltd., Faculty of Science, Chulalongkorn University, Bangkok 10330 Thailand

*Corresponding author, e-mail: vtirayut@chula.ac.th

Received 15 Jan 2025, Accepted 30 Apr 2025
Available online 28 May 2025

ABSTRACT: Styryl-cyanine dyes, a class of conjugated organic molecules, have emerged as essential tools in bioimaging due to their exceptional optical properties. This review highlights recent advancements in the development of these dyes for bioimaging nucleic acids, cellular organelles, and proteins. Key molecular design strategies for developing target-specific probes and an overview of synthesis approaches, mechanisms of action, and biomolecular interactions are discussed. These insights underscore the versatility and critical role of styryl-cyanine dyes in advancing bioimaging technologies, offering enhanced capabilities for visualizing and understanding complex biological processes in living cells at the molecular levels.

KEYWORDS: styryl-cyanine dyes, staining dyes, fluorescence imaging, nucleic acid bioimaging, bioimaging of cellular organelles, protein bioimaging

INTRODUCTION

Bioimaging has become an indispensable technique for investigating living cells — the fundamental units of life — and understanding complex biological processes within them. Such understanding provides valuable insights that can drive the development of new diagnostic and therapeutic approaches. Suitable imaging agents tailored to specific applications enable effective bioimaging. Apart from selectively interacting with the desired target to be visualized and possessing convenient excitation and emission wavelengths, ideal imaging agents should also exhibit the following characteristics: ability to penetrate the membranes to reach the target, low cytotoxicity, and photostability. Consequently, developing novel dyes with the abovementioned desirable properties has attracted significant attention from researchers. In recent years, fluorescent organic dye molecules, typically highly conjugated aromatic compounds, have emerged as key tools for bioimaging. Their structures can be flexibly designed to achieve desirable physicochemical, biological and optical characteristics while maintaining low toxicity.

Cyanine dyes (Fig. 1) are highly conjugated organic molecules characterized by the presence of two nitrogen atoms, one bearing a positive charge and the other remaining neutral. A polymethine bridge connects these nitrogen atoms with an odd number of conjugated carbon atoms. The nitrogen atoms in cyanine dyes may exist in an open-chain configuration or be incorporated into heterocyclic structures such as pyrrole, imidazole, thiazole, pyridine, quinoline,

indole, and benzothiazole. When only one of the nitrogen atoms is part of a heterocyclic ring, the resulting structure is classified as a hemicyanine dye [1].

Styryl dyes are a class of conjugated organic molecules featuring the styryl group (Ar–CH = CH–) connected to another aromatic ring system. In typical styryl dyes, one of the aromatic rings is electron-rich, and another is electron deficient, thereby creating a donor- π -acceptor or push-pull system which is fundamental for its unique optical properties (Fig. 1). The electron-deficient part is frequently a heteroaromatic group such as pyridine, benzothiazole or quinoline. In such cases, the molecule shares structural similarities with cyanine dyes and is often referred to as styryl-cyanine or styryl-hemicyanine dyes [2].

Styryl-cyanine dyes have been known for more than a century. Historically, they have been developed as sensitizers for photographic applications [3]. The ease of synthesis, tunable structure and optical properties, and good photostability make these dyes useful for many other applications, including laser dyes [4], dye-sensitized solar cells [5], optoelectronic devices [6], and non-linear optical materials [7]. More recently, they have been widely used as histological stains [8], fluorescent chemosensors [9–12], probes for specific enzyme activity [13, 14], as well as for biomolecules such as nucleic acids and proteins [15]. Previous reviews on styryl dyes and their applications were published over ten years ago [2, 16]. Another recent review emphasizes the synthesis of styryl dyes for application in non-linear optical (NLO) materials [17]. This review aims to focus on recent advancements in the molecular design of styryl-cyanine dyes with a donor- π -acceptor configuration, with special emphasis

[†]2014 Outstanding Scientist of Thailand; Editorial Board of *ScienceAsia*, 2019–present.

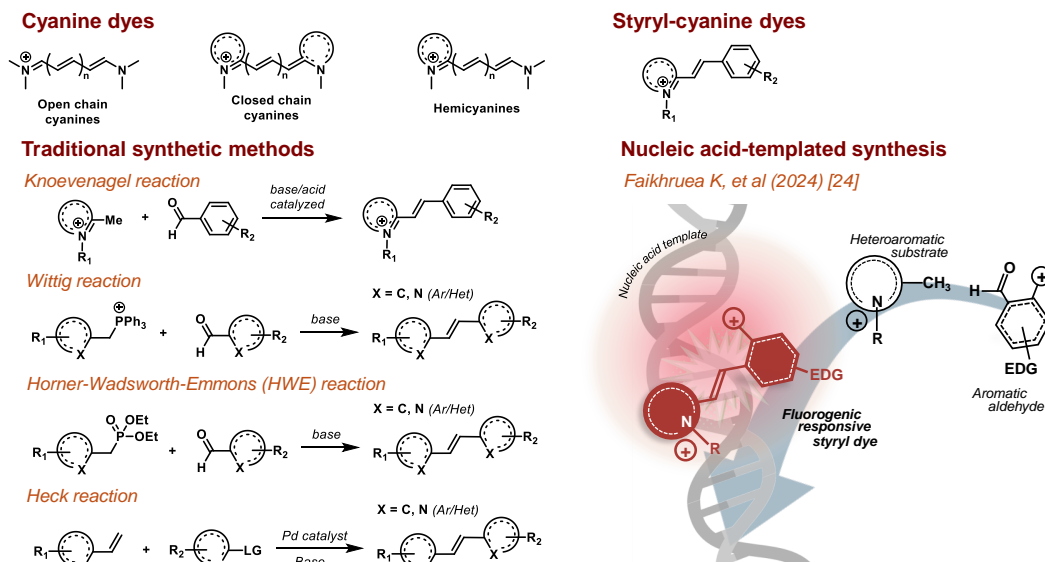


Fig. 1 Generic structures and synthesis strategies of styryl-cyanine dyes.

on visualization and bioimaging of macromolecular components in the cells, including nucleic acids, cellular organelles, and proteins. The detection of ions and small molecule targets is not included to keep the review concise and focused. Even with such a limited scope, the review is not meant to be comprehensive but to highlight selected recent advancements in the field and showcase contributions from our group to this critical research area.

SYNTHESIS STRATEGIES

The synthesis of styryl-cyanine dyes is most commonly achieved through the Knoevenagel-type condensation, whereby an activated methyl or methylene group reacts with an aromatic aldehyde to form the styryl linkage. Typically, the dye could be straightforwardly synthesized by heating a heterocyclic building block bearing an activated methylene or methyl group with an aromatic aldehyde in the presence of acetic anhydride [15] or piperidine [18].

The Wittig reaction offers an alternative approach for synthesizing styryl-linked organic compounds. In this process, an aldehyde or ketone reacts with an ylide, produced from a phosphonium salt, forming styryl-based compounds [11, 19, 20]. Relating to this, the Horner-Wadsworth-Emmons (HWE) reaction has also been employed to synthesize styryl dyes. This reaction involves the formation of an alkene product

through the reaction of a phosphonate-stabilized carbanion with an aldehyde or ketone [21]. Alternatively, styryl dyes have been successfully synthesized via the Heck reaction [22, 23]. This method involves coupling an aryl halide or triflate with an alkene in the presence of a palladium catalyst and a base to form a substituted alkene.

Apart from these traditional approaches, a novel synthesis of styryl dyes utilizing nucleic acid-templated synthetic reactions has been recently developed by our research group [24]. This strategy involves two key coupling partners (a heteroaromatic system with an active methyl group and an aromatic aldehyde), which bind to a DNA or RNA template. Due to the proximity effect, the nucleic-acid-bound starting materials efficiently reacted, generating the styryl dye product in its template-bound form under mild conditions. This approach accelerates styryl dye synthesis and allows direct evaluation of the optical properties of the resulting dyes. Furthermore, the method enables the screening of suitable coupling partners that selectively bind to specific nucleic acid structures such as G-quadruplexes. The synthesis strategies of the styryl-cyanine dyes are summarized in Fig. 1.

Mechanisms of fluorescence change

The asymmetric donor- π -acceptor (D- π -A) configuration of the styryl-cyanine dyes, often described as a

push-pull system, is responsible for their intriguing optical properties. Due to their dipolar nature, these properties are highly influenced by environmental factors such as solvent polarity and viscosity. The solvatochromic behavior of these dyes in solution can be understood by comparing their permanent dipole moments. When the excited state has a higher dipole moment than the ground state, polar solvents preferentially stabilize the excited state, reducing the energy gap between the two states. This results in a red-shifting of both the absorption and emission spectra [25].

Furthermore, the styryl-cyanine dyes are classified as molecular rotors due to their ability to adopt twisted conformations, where one part of the molecule rotates relative to the rest upon excitation. This behavior is associated with a process known as twisted intramolecular charge transfer (TICT), a characteristic feature of this class of fluorophores. After absorbing a photon, a molecular rotor can return to its ground state through two possible pathways: from the locally excited (LE) state or the twisted state. The energy gaps between the LE, twisted, and ground states differ significantly. De-excitation from the twisted state typically leads to either a red-shifted emission wavelength or a complete absence of fluorescence. The non-radiative relaxation pathway is prohibited if the molecular motion is restricted, such as through binding to a host molecule or in solvents with high viscosity, thereby increasing fluorescent quantum yield, as illustrated in Fig. 2a [26].

Another mechanism that affects the fluorescence of styryl dye molecules is the aggregation-induced emission (AIE). This phenomenon occurs due to the restriction of intramolecular rotation (RIR) in the aggregated form of dyes, which limits nonradiative decay pathways and results in strong fluorescence emission [27–29].

INTERACTION WITH BIOLOGICAL MOLECULES

Binding to nucleic acids, organelles and proteins

Noncovalent binding modes of small molecules to nucleic acid targets are classified into three major types, as depicted in Fig. 2b. The first binding mode is electrostatic interaction, where the negatively charged phosphate backbones of nucleic acids attract positively charged dyes, enabling sequence-independent binding to the nucleic acid strands. Another common interaction found in planar aromatic or heteroaromatic planar dye molecules is intercalation. In this process, the planar dye molecules are inserted and stacked between the base pairs of DNA duplexes. The molecules are oriented perpendicular to the helix axis, leading to the elongation of the DNA duplex. Specific small molecules can also bind to the minor groove of DNA duplexes. The molecules are often crescent-shaped and interact with DNA by forming

hydrogen bonds with the base pairs, thereby stabilizing the DNA-ligand complex [30]. Typical intercalators (such as ethidium and acridine orange) and groove binders (DAPI, Hoechst 33342) also carry one or more positive charges to enhance the interaction with DNA via electrostatic attraction with the negatively charged phosphate groups in the DNA.

The binding of styryl dyes to nucleic acids restricts their conformational mobility, thereby enhancing fluorescence, as discussed above. Simple pyridinium-based styryl dyes such as *trans*-4-[4-(dimethylamino)styryl]-1-methylpyridinium iodide (DSMI, also known as DASPMI or 4-D-1-ASP; Fig. 2c) binds to dsDNA via the minor groove binding mode which is accompanied by a modest increase in fluorescence emission (up to 10-fold) [31]. However, the intercalating mode is possible for styryl dyes bearing larger aromatic groups [32, 33]. Unlike those in the monostyryl structures, it was observed that styryl dyes with bisstyryl structures are shown to aggregate along the minor groove of DNA [34].

For effective organelle staining, the molecular design should incorporate cell-permeable abilities and organelle-targeting groups that are selectively tailored to each organelle's unique characteristics (Fig. 2d) [35, 36]. A list of common organelle-targeting groups is summarized in Table S1. The mitochondrial membrane potential is characterized by a negative voltage of approximately -180 mV, which facilitates the permeation of lipophilic, positively charged molecules into the mitochondria. In the case of lysosomes, the lumen maintains an acidic environment with a pH of around 4.5, making lipophilic amines suitable as probes for lysosomal targeting [37]. For the cell membrane, probe molecules require membrane-anchoring moieties, such as long-chain hydrocarbons or cholesterol, to reduce diffusion and maintain their localization within the membrane.

Aggregated proteins are widely used as biomarkers for diagnosing many early-stage disorders [38]. For protein detection using molecular rotors, the dye molecule is placed at the interface of two interacting proteins, where fluorescence is activated due to restricted molecular rotation (Fig. 2e). Desirable probes should be able to distinguish between monomeric and aggregated protein forms, even at similar quantities or concentrations.

APPLICATIONS OF STYRYL DYES IN BIOIMAGING

Nucleic acids

Nucleic acids are vital biomolecules in living organisms, playing a key role in transmitting genetic information to the next generation and regulating protein synthesis. Any abnormalities in nucleic acid production can result in genetic disorders or defects, often due to the production of atypical or malfunctioning proteins. Styryl-cyanine dyes have been extensively

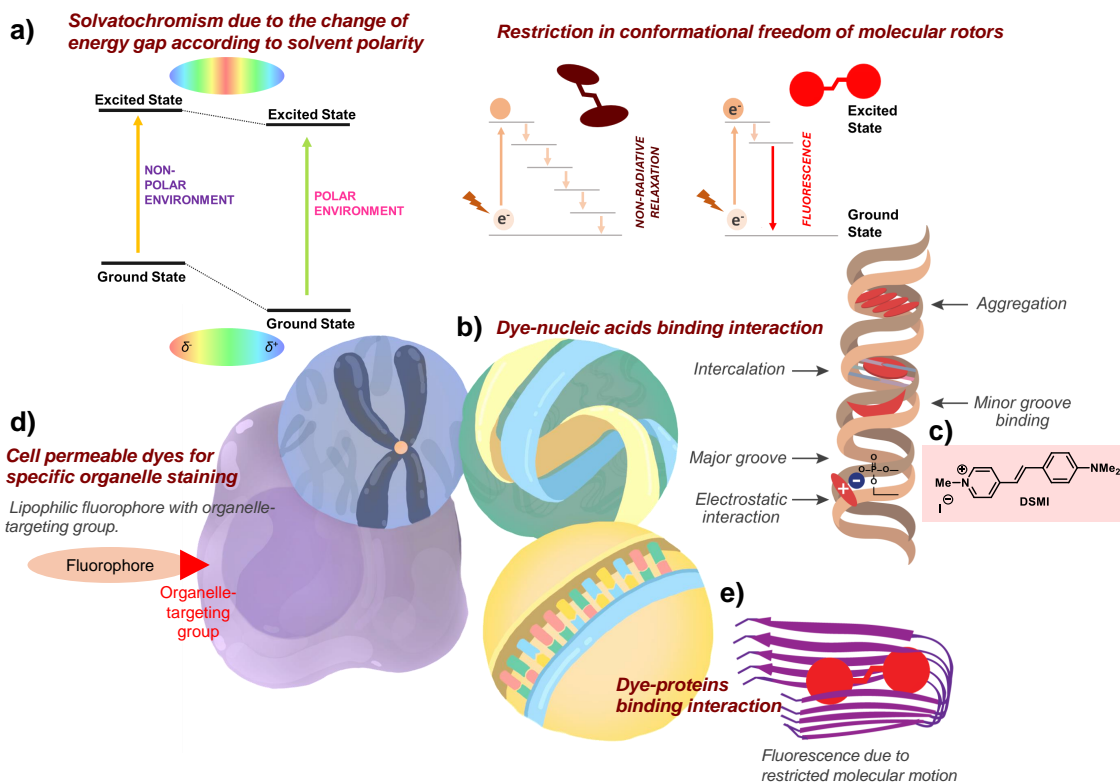


Fig. 2 Binding interactions to biomolecules and mechanisms of fluorescence changes in styryl dyes.

utilized as nucleic acid probes due to their remarkable optical property changes upon target binding. Researchers continue to focus on advancing these dyes to enhance their sensitivity and selectivity for nucleic acid targets. Strategies to improve dye performance aim to increase binding affinity to target nucleic acids, enhance specificity for particular nucleic acid types or structures, and investigate molecular structures that selectively recognize specific nucleobase sequences. This section primarily highlights recent advancements in the development and application of styryl-cyanine dyes for detecting RNA, double-stranded DNA, and G-quadruplex secondary structures in guanine-rich DNA, with special emphasis on cellular nucleic acids bioimaging.

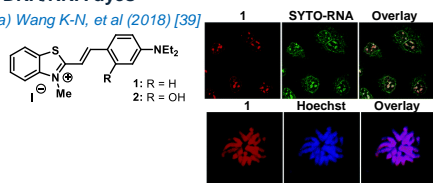
Styryl cyanine dyes have been extensively used for the bioimaging of cellular nucleic acids and related cellular structures such as ribosomes, nucleoli, and chromosomes. Selected recent examples of nucleic acid probes based on styryl-cyanine dyes are presented in Table S2. In one example, simple cationic styryl benzothiazolium dyes (Fig. 3a) were employed to visualize the nucleolus during interphase and chromosomes during mitosis, offering detailed insights into the cell

cycle without affecting cell viability [39]. Further from bioimaging, two DNA-responsive styryl-cyanine dyes featuring an *N*-ethylated indole linked to either quinolinium (Styryl-QL) or benzothiazolium (Styryl-BT) (Fig. 3b) demonstrated significant anti-bacterial and anti-cancer properties. These findings highlight the styryl-cyanine dyes' dual utility in bioimaging and therapeutic fields [40]. In our recent study, an additional positive charge was introduced into the cationic styryl dye molecules to enhance their binding affinity to nucleic acids (Fig. 3c). This design strengthens binding to target nucleic acids through electrostatic interactions with the negatively charged phosphate backbone [32]. These dicationic styryl dyes exhibited significantly higher affinity for double-stranded DNA (dsDNA) and produced stronger fluorescence and colorimetric responses than monocationic dyes. They were successfully applied for the *in vitro* detection of bacterial DNA, serving as a prototype for point-of-care platforms for foodborne pathogen detection [32, 41]. Applications for cellular nucleic acids imaging were also demonstrated in HeLa cells, whereby cellular RNA and nucleoli were found to be the primary target [32].

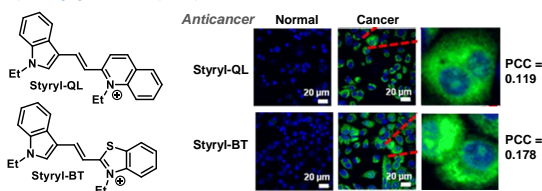
Unless anchored on another sequence-specific

DNA/RNA dyes

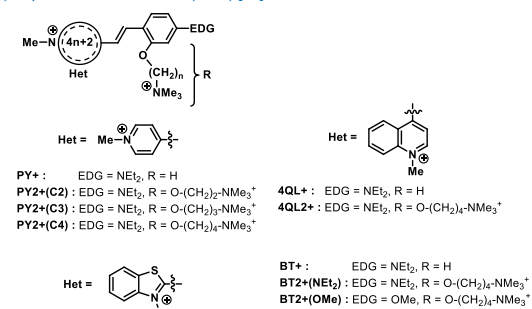
a) Wang K-N, et al (2018) [39]



b) Wangngae S, et al (2023) [40]



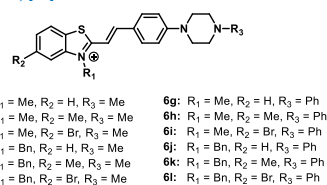
c) Supabowornsathit K, et al (2022) [32]



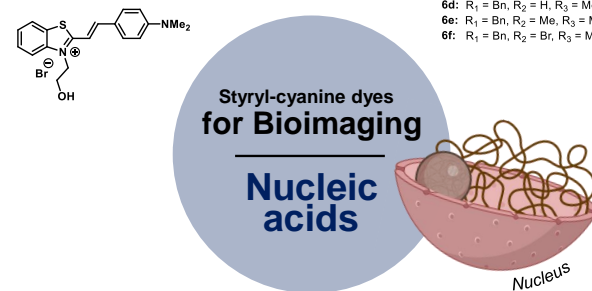
Antibacterial

Compound	MIC (µg mL ⁻¹)	
	<i>E. coli</i> 780	<i>S. aureus</i> 1466
Styryl-QL	4 ± 0.005	4 ± 0.002
Styryl-BT	16 ± 0.001	1 ± 0.005

d) Zonjić I, et al (2022) [44]

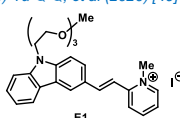


e) Patidar RK, et al (2023) [45]

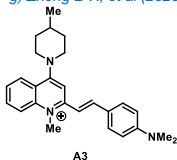


G-quadruplex DNA selective dyes

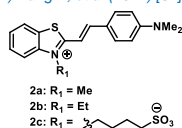
f) Yu Q-Q, et al (2020) [49]



g) Zheng B-X, et al (2020) [50]

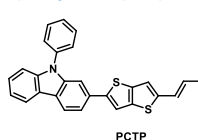


h) Kang Y, et al (2022) [51]

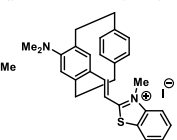


RNA selective dyes

i) Jiang C, et al (2023) [52]



j) Felder S, et al (2022) [21]



k) Fang L, et al (2022) [53]

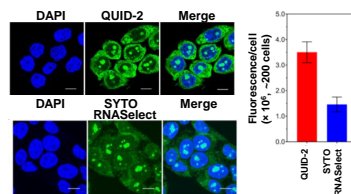
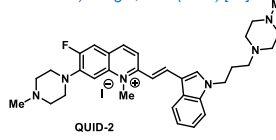


Fig. 3 Bioimaging of nucleic acids using styryl-cyanine dyes. Figs. 3a, 3b, and 3k were adapted from Refs. [39], [40], and [53], respectively. Fig. 3a is reproduced with permission from the Royal Society of Chemistry. Figs. 3b and 3k are published under the Creative Commons Attribution License (CC BY).

probe [42, 43], styryl cyanine dyes tend to bind indiscriminately to dsDNA without sequence selectivity. However, the benzothiazolium-based styryl dyes with *N*-methylpiperazinyl aromatic substituents exhibited a pronounced fluorescence response with AT-rich DNA sequences (Fig. 3d). These dyes demonstrated pref-

erential binding to the AT-minor groove, notable stabilization of the double helix, and positive induced circular dichroism spectra [44]. In the same study, a related dye with the *N*-phenyl substituent showed a strong affinity for the Tel22 DNA G-quadruplex, albeit with only a modest fluorescence response. In another

report, the fluorescence of a benzothiazolium-based styryl dye with a hydroxyethyl appendage (Fig. 3e) was selectively enhanced in the presence of oncogene promoter G-quadruplexes sequences. In contrast, negligible or weak fluorescence enhancement was observed with ssDNA, dsDNA, and RNA [45]. Although a detailed understanding of such selectivity at the molecular level is still missing, these results suggest possibilities for development of styryl dyes that show selective binding or responsiveness to specific nucleobase sequences or secondary structures of interest.

Due to the perceived crucial biological roles of DNA G-quadruplexes (GQ) [46, 47], the development of fluorescent GQ-DNA probes for theranostic applications has been emerging in recent years [48]. The approach to increase specificity towards G-quadruplex secondary structures is to introduce a side group on the core unit of the dye structure to increase molecular rigidity. For instance, the styryl dye with pyridinium core structure conjugating with the carbazole scaffold through an ethylene bridge (E1, Fig. 3f) possessed excellent selectivity towards G-quadruplex DNA over duplex DNA and other biologically relevant molecules with fluorescent turn-on signal [49]. Another example involves a quinolinium-based dye with a dimethylamino aromatic substituent, where the introduction of a methylpiperidine side group to the quinolinium core significantly enhanced its selectivity for the quadruplex structures of c-myc pu27 (A3, Fig. 3g). The dye also exhibited high binding affinity toward these G-quadruplex structures [50]. According to a 2022 study, the affinity and fluorescence response of benzothiazolium-based styryl-cyanine dyes to different G-quadruplex DNA structures is determined by the charge and length of the side chain groups attached to the nitrogen atom of the benzothiazolium core. The results revealed that dyes with *N*-methyl and *N*-ethyl side chains displayed higher affinity for G-quadruplex DNA compared to the anionic sulfonate side chain (Fig. 3h). Notably, the dye with an *N*-ethyl side chain could induce conformational changes in both bcl-2 and KSS G-quadruplexes. Furthermore, all the compounds investigated in this study promoted the folding of bcl-2 from a coiled structure to a hybrid G-quadruplex form [51].

Dyes that can distinguish RNA from DNA are typically designed with non-coplanar aromatic moieties. These structures facilitate selective interaction with RNA secondary structures via π -stacking while minimizing undesirable intercalation or groove binding with DNA. For instance, the dye (*E*)-4-(2-(5-(9-phenyl-9*H*-carbazol-2-yl)thieno[3,2-*b*]thiophen-2-yl)vinyl)-1-propylpyridin-1-ium (PCTP) (Fig. 3i) was developed using 9-phenylcarbazole as an electron donor and a pyridinium heteroaromatic as an electron acceptor. Incorporating a thieno[3,2-*b*]thiophene unit extends the π -conjugation, enhances

intramolecular charge transfer (ICT), and induces a red shift in the fluorescence emission peak. This design enables the dye to distinguish RNA from DNA in solution and cells, exhibiting high selectivity and sensitivity toward RNA [52].

Furthermore, the design of three-dimensional ligands (3D ligands), which are non-coplanar aromatic structures capable of engaging with RNA secondary structures via π -stacking while minimizing nonspecific intercalation or groove binding, offers a promising approach to improving RNA selectivity. In 2022, a [2.2]paracyclophane (pCp) moiety was incorporated into the nonselective 2-(4-dimethylamino-styryl)-3-methyl-benzothiazolium styryl dye (Fig. 3j). The replacement of the phenyl ring with the pCp unit resulted in a dye with significantly higher RNA selectivity compared to the traditional nonselective dye [21]. In addition to structural modifications, selective staining of RNA dyes can be achieved through enzyme-digestion-based screening. This method involves staining cells with the studied compounds, followed by enzymatic digestion of cellular DNA and RNA using DNase and RNase, respectively. Fluorescent probes with RNA specificity exhibit a loss of fluorescence after RNase treatment, while no significant change is observed following DNase treatment. A recent study [53] reported a new RNA-specific styryl dye based on a hit compound identified through the enzyme-digestion screening assay in their previous research [54]. The hit compound obtained from this study, QUID-2 (Fig. 3k), demonstrated superior performance compared to the commercially available RNA staining probe, SYTO RNaselect. It exhibited high selectivity, enhanced sensitivity, low cytotoxicity, and excellent photostability. A similar enzymatic digestion strategy has demonstrated that cellular RNA acted as a template for styryl dye formation in living cells instead of DNA [24].

Organelles

Organelles staining is essential for studying cell dynamics and functionality. However, the availability of commercially produced dyes that specifically target particular organelles remains limited, and their use often requires technical expertise. As a result, researchers have been actively developing novel staining agents that can selectively label specific organelles while minimizing cytotoxicity. Styryl-cyanine dyes have emerged as a promising class of staining dye for this purpose. This section focuses on recent progress in developing and applying styryl-cyanine dyes for selective staining of cellular structures, including mitochondria, lysosomes, cell membranes, and stress granules. Selected recently developed dyes for visualizing specific cellular organelles are summarized in Table S3.

Molecular design strategies to achieve selective binding to specific organelles often involve incorpo-

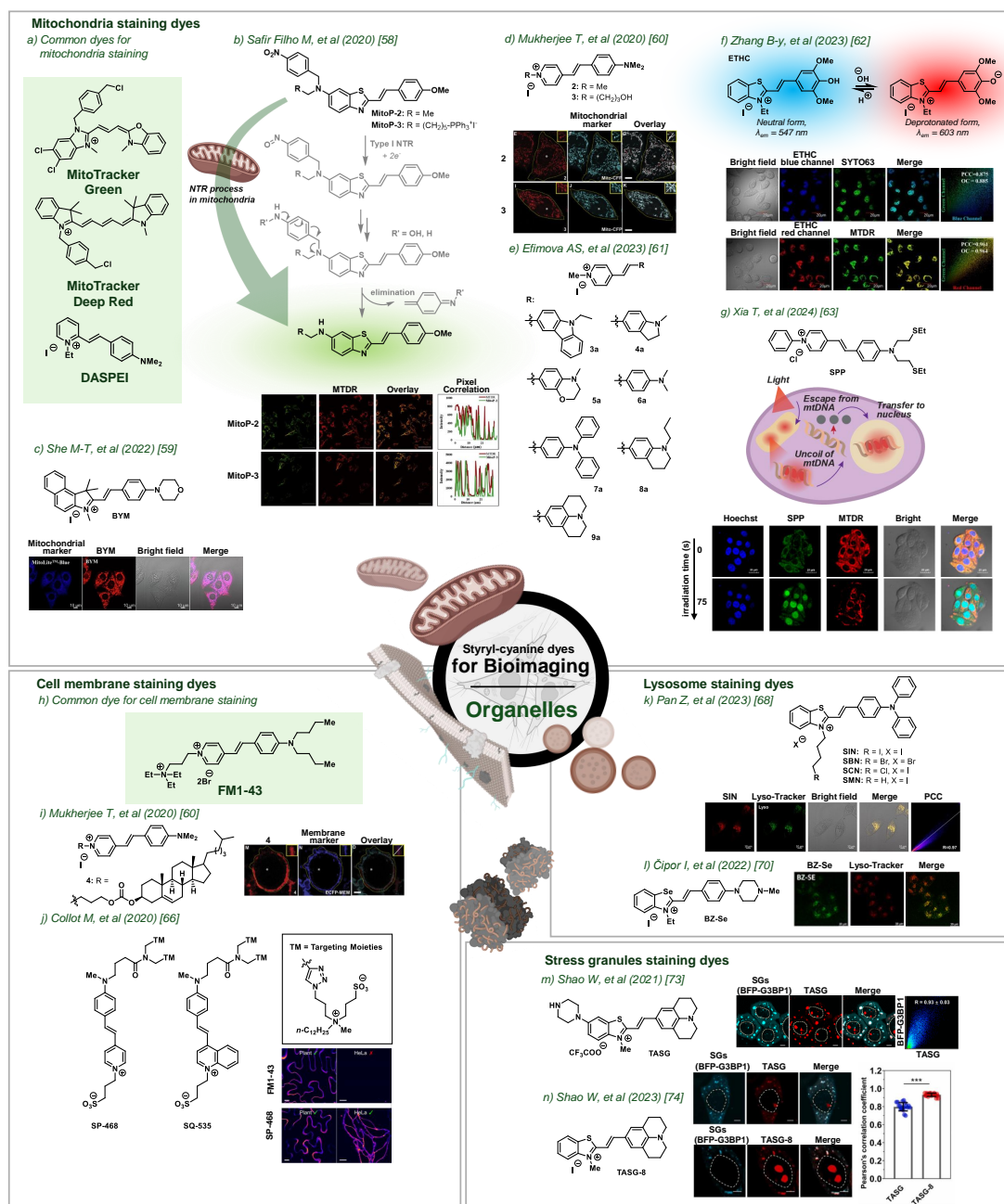


Fig. 4 Bioimaging of cellular organelles by styryl-cyanine dyes. Figs. 4b, 4c, 4d, 4f, 4i, 4k, 4l, and 4n are adapted from Refs. [58], [59], [60], [62], [60], [68], [70], and [74], respectively, with permission from Elsevier (copyright Elsevier B.V.). Figs. 4g, 4j and 4m are adapted from Refs. [63], [66] and [73], respectively, with permission (copyright American Chemical Society).

rating known targeting groups or introducing specific structural modifications within the fluorophore skeleton. The net negative membrane potential across the mitochondrial matrix is exploited for mitochondria staining using fluorescent probes with a net positive charge [37].

Positively charged cyanine dyes such as MitoTracker Green and MitoTracker Deep Red (Fig. 4a) have been widely utilized as effective staining agents for mitochondria. The compound *trans*-2-(4-(dimethylamino)styryl)-1-ethylpyridinium iodide

(DASPEI) is a representative styryl dye that has been used to stain mitochondria of live cells and measurements of mitochondrial membrane potentials [55]. The mitochondrial accumulation depends on the membrane potential and is accompanied by a substantial fluorescence enhancement. Fluorescence lifetime measurement suggested the partial insertion of the DASPEI molecule in the outer leaflet of the inner mitochondrial membrane with polar methylpyridinium moiety favors interactions with the outer leaflet, leaving the hydrophobic aniline moiety aligns with lipid hydrocarbon chains [56].

Many research groups have subsequently developed mitochondria-targeting styryl-cyanine dyes with structural similarities. For instance, a styryl pro-fluorescence probe with a 4-nitrobenzyl masking group was designed to visualize mitochondria based on the specific action of the mitochondrial nitroreductase (NTR) enzyme [57]. In this case, the dyes with or without the triphenylphosphonium as a mitochondria-targeting group (MitoP-3 or MitoP-2, Fig. 4b) performed equally well, indicating that the NTR activity alone is sufficient for precise targeting of mitochondria [58]. In 2022, a novel mitochondria-specific fluorescent turn-on probe (BYM, Fig. 4c) was developed, featuring a benzo-indole core with a *p*-morpholino-substituted styrene moiety. [59]. The probe exhibited high photostability and selectively targeted mitochondria without entering the nucleus, as demonstrated by cell imaging studies. Furthermore, the pyridinium core structure has been recognized as a key component for efficient mitochondrial targeting. This finding has been further supported by recent studies (Fig. 4d,e) [60, 61], where dyes incorporating a pyridinium group demonstrated mitochondria-specific localization capabilities.

Due to their excellent nucleic acid staining ability, styryl-cyanine dyes may also penetrate the nucleus and exhibit a fluorescent response to nucleic acids in the nucleus. Selective localization of the dye between the nucleus and mitochondria could be achieved and demonstrated radiometrically by a styryl dye bearing a benzothiazolium moiety linked to a 4-hydroxy-3,5-dimethoxystyryl group (ETHC, Fig. 4f). This design leverages the pH-responsive nature of the phenolic hydroxyl group, which exhibits two distinct major absorption bands under acidic (neutral form) and basic conditions (deprotonated form). As a result, two excitation channels corresponding to low and high pH environments were established, enabling differential staining of organelles with varying pH characteristics. Since the nuclear matrix is acidic and the mitochondrial matrix is basic, the dye can permeate both organelles, as confirmed by colocalization experiments with commercial organelle-specific staining dyes. In the acidic environment of the nucleus, the dye exists in a protonated form, requiring a lower excita-

tion wavelength (blue channel). Conversely, under the basic environment of the mitochondria, the dye adopts a deprotonated form, allowing excitation at a higher wavelength (red channel). This dual-staining capability facilitates precise localization of the dye in cells, enabling distinct visualization of organelles with different pH profiles. Additionally, the developed dye offers the ability to track pH changes in mitochondria, providing a potential tool for detecting cellular abnormalities linked to pH fluctuations. This capability opens new avenues for diagnostic applications related to mitochondrial dysfunction and cellular homeostasis [62].

In an advanced example, a dye capable of migrating from mitochondria to the nucleus upon light stimulation was reported [63]. The SPP probe (Fig. 4g) was designed by incorporating an *N*-arylpiperidine unit, a positively charged DNA-affinity group, onto one side of the styryl skeleton to enhance DNA selectivity and promote mitochondrial accumulation. A bis(2-(ethylsulfanylethyl)amino) group was introduced as an aromatic substituent to increase steric hindrance within the DNA grooves. This structural modification enables the dye to dissociate from mitochondrial DNA (mtDNA) when the internal stress of the DNA double helix is relieved upon exposure to visible light, driving its migration from the mitochondrion to the nucleus.

The lipid bilayer structure of the cell membranes consisted of hydrophilic phospholipid heads and hydrophobic tails. The commercially available styryl-based FM dye family, such as FM1-43 (Fig. 4h), introduced in the early 1990s, is widely used for cell membrane staining and visualizing dynamics processes such as membrane internalization and endosome recycling [64, 65]. The dye suffers certain limitations, such as the lack of affinity and inefficient staining in fixed cells, susceptibility to internalization by endocytosis, and broad absorption and emission spectra. Nevertheless, favourable optical properties and high photostability of the dye suggest that it could be a prototype for further development. To create dyes specific to cell membranes, membrane-anchoring moieties, such as long alkyl chains or biomolecules like cholesterol, must be incorporated into the dye molecule. This design minimizes the diffusion of the probe into the cells. In 2020, a styryl dye bearing a pyridinium group tethered with cholesterol successfully targeted the cell membrane and showed strong interaction with liposomes (Fig. 4i) [60]. Moreover, the design of neutral zwitterionic dyes with long amphiphilic groups was shown to enhance the cell membrane marker performance by reducing cross-talk and improving the brightness as well as the photostability while maintaining high membrane affinity for various cell types (Fig. 4j) [66].

For lysosome staining, lysosome-specific probes are often designed to include a basic amine functionality such as the dimethylaminoethylamide group,

which serves as a targeting moiety to direct the fluorophore toward the acidic lysosomal lumen (pH 4.5) [37]. In addition, the benzothiazolium group itself had also been proven to be a lysosome-targeting group [67]. Thus, novel lysosome-targeting styryl-cyanine dyes with a benzothiazolium core and triphenylamine group were developed, and they exhibited precise lysosomal targeting in HeLa cells (Fig. 4k) [68]. Furthermore, these dyes could generate singlet oxygen upon irradiation, making them potentially useful for photodynamic therapy. The introduction of selenium atom has been demonstrated to play an important role in lysosome targeting. In 2020, a specific localization in lysosomes of an indolenium-based hemicyanine dye containing a xanthene-phenyl-seleno aromatic moiety was reported. In addition, the dyes also exhibit viscosity-dependent fluorescence, making them applicable to monitor changes in lysosomal viscosity [69]. Another subsequently developed benzo[d][1,3]selenazole styryl dye (BZ-Se, Fig. 4l) demonstrated preferential localization in lysosomes while the corresponding benzo[e]indole-dye distributed equally in mitochondria and lysosomes [70]. These results further confirmed the crucial role of the selenium atom in facilitating lysosome-specific targeting.

Stress granules (SGs) are membrane-less organelles in eukaryotic cells formed by a congregation of RNA-protein binding via liquid-liquid phase separation when translation initiation is restricted. In recent years, SGs have attracted extensively because of their vital signaling and cellular response, such as oxidative stress, heat shock, or viral infection. Hence, powerful tools for investigating the assembly, disassembly, or dynamic changes of SGs in cells have emerged. Traditionally, immunofluorescence and fluorescence *in situ* hybridization (FISH) are utilized, but the high cost and unsuitability for live-cell monitoring limit these techniques [71, 72]. Over the past decades, a few styryl-cyanine dyes have been developed as small organic fluorescent probes for SG imaging. In 2021, TASG, a styryl-cyanine dye featuring a piperazinyl-substituted benzothiazolium core linked to a julolidine aromatic unit, was successfully established (Fig. 4m) [73]. The dye exhibited weak fluorescence in non-stressed HeLa cells but concentrated in and lit up after SGs formation under stress conditions. The dye showed strong fluorescence co-localization with the reference SG marker blue fluorescent-G3BP1 with excellent Pearson's coefficient. However, due to its steric structure, TASG faced limitations in visualizing small nascent SGs and monitoring SG dynamics in live cells. Subsequently, the same group developed a modified version of TASG, named TASG-8, by removing the piperazinyl group from the benzothiazolium unit (Fig. 4n) [74]. TASG-8 exhibited superior performance compared to TASG, effectively labeling small nascent

SGs with improved clarity.

Protein aggregates

Numerous fluorescence dyes have been developed to detect protein aggregation, which serves as a potential marker for frontotemporal dementia and other neurodegenerative diseases. Traditionally, the commercially available molecular rotors Thioflavin S (ThS) and Thioflavin T (ThT) dyes are widely used to visualize protein aggregates, including those linked to neurodegenerative disorders such as Alzheimer's disease [75]. However, their short emission wavelengths (500–550 nm) present a significant drawback, as autofluorescence in biological tissues can interfere with the fluorescence signals, making them less suitable for deep-tissue imaging. Furthermore, these emission wavelengths overlap with conventional nuclear staining dyes such as DAPI [76]. Thiazole Orange (TO), a well-known cyanine dye initially developed for DNA staining purposes, has been identified as an effective amyloid marker owing to its significant fluorescence enhancement upon binding to amyloid fibrils. This enhancement results from restricted intramolecular rotation and intermolecular dye aggregation [77]. The structures of common dyes for amyloid bioimaging are illustrated in Fig. 5a. The quinolinium and benzothiazolium units, derived from the core structures of Thioflavin and Thiazole Orange, along with structurally related derivatives such as benzoxazolium and indolenium moieties, have thus emerged as the frameworks for subsequent development of novel dyes used in amyloid protein detection. Representative examples of dyes showcased in this review are included in Table S4.

Several styryl-cyanine dyes have been reported as promising agents for detecting amyloid protein aggregates [19, 78, 79]. Compared with ThT, the styryl-cyanine dye structure incorporates an extra double bond between the acceptor thiazolium salt and donor dialkylaminophenyl units. The extended π -conjugation contributes to the red-shifting of the emission spectra and also introduces an additional rotational degree of freedom to enhance the difference in fluorescence quantum yields between rigid and aqueous environments. In 2021, two benzothiazolium-based styryl dyes with piperidinyl and methylpiperazinyl aromatic substituents were reported (RB1 and RB2, Fig. 5b). The piperidinyl-substituted styryl dye (RB1) exhibited significantly improved properties compared to the conventional ThT dye. It demonstrated a 76 nm red shift in absorption maxima and a 112-fold increase in fluorescence upon binding to amyloid fibrils, along with a stronger binding affinity for α -synuclein fibrils. These attributes make it highly suitable for imaging intracellular α -synuclein fibrils with minimal cytotoxicity. The dye RB2, featuring a methylpiperazinyl aromatic substituent, exhibited a

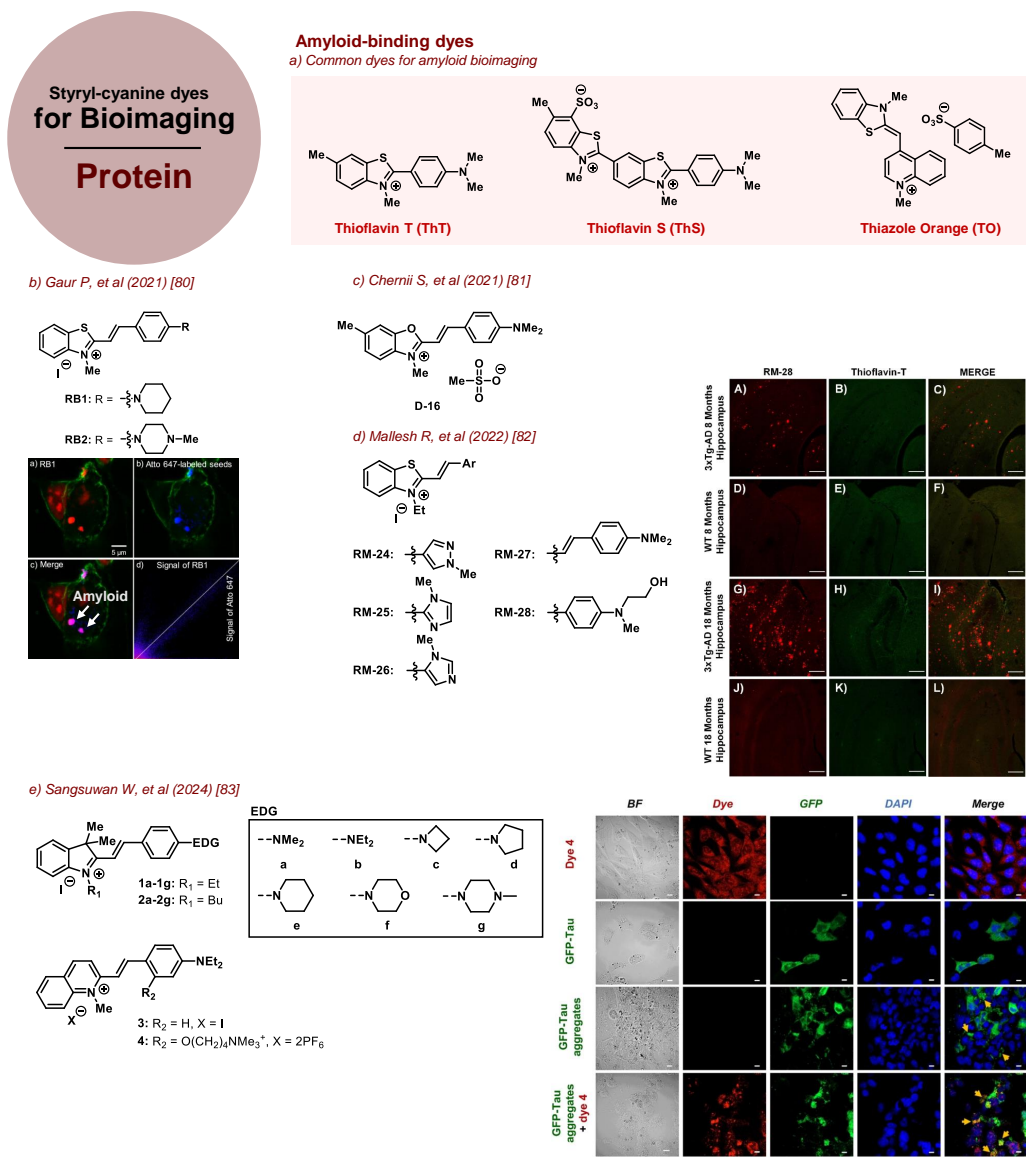


Fig. 5 Bioimaging of protein aggregates by styryl-cyanine dyes. Figs. 5b and 5d are reproduced with permission from Refs. [80] and [82], respectively (copyright American Chemical Society), and Fig. 5e is reproduced with permission from Ref. [83] (copyright John Wiley & Sons, Inc.).

lower affinity for α -synuclein fibrils than RB1, but it still outperformed the ThT dye [80].

In 2021, a benzoxazolium-based styryl dye with dimethylamino aromatic substituent (D-16, Fig. 5c) was identified as a specific probe for detecting pathological amyloid fibrils, particularly those of β -lactoglobulin. The dye demonstrated higher selectivity against other biomolecules, including monomeric insulin, amyloid fibrils of insulin, monomeric beta-lactoglobulin, monomeric lysozyme, fibrillar lysozyme,

bovine serum albumin, as well as low- and high-molecular-weight DNA [81].

In 2022, a series of styryl dyes (RM-24 to RM-28, Fig. 5d) with an *N*-ethylated benzothiazolium core was developed for the selective detection of amyloid beta ($A\beta$) aggregates associated with Alzheimer's disease [82]. Among them, RM-28 emerged as the most effective fluorescent probe, demonstrating strong affinity and high sensitivity (7.5-fold fluorescence increase). It can efficiently cross the blood-brain barrier in mice and

was successfully used to detect A β aggregates in 3xTg-AD brain sections and *in vitro* assays. Notably, RM-28 exhibits high specificity for A β aggregates, showing no binding to intracellular proteins like bovine serum albumin (BSA) or α -synuclein (α -Syn) aggregates.

Our group recently reported a new set of styryl-cyanine dye derivatives with the quinolinium and indolenium core structures (Fig. 5e) and studied their interactions with tau aggregates *in vitro* and living cells. The dye 4, which incorporates a quinolinium moiety with two cationic sites, showed a significant 28-fold increase in fluorescence when bound to tau aggregates. It also successfully stained tau aggregates in living cells, as confirmed by confocal fluorescence microscopy. A molecular docking study further supported these binding interactions [83].

CONCLUSION AND FUTURE PERSPECTIVES

In conclusion, styryl-cyanine dyes play a significant role in bioimaging technologies, with proven utility in visualizing nucleic acids, organelles, and proteins. This review highlights their versatility, recent advancements, and underlying molecular design principles. Future developments could focus on structural functionalization to enhance biomolecular specificity, reduce off-target interactions, improve photophysical properties for high-resolution and deep-tissue imaging, and tailor dyes for disease diagnostics and dynamic cellular monitoring. Diversity-oriented synthesis or rational design, driven by deep molecular understanding and computational modeling or AI, will contribute to achieving these challenging goals. Additionally, integrating dual-function capabilities, such as combining imaging with therapeutic applications or switchable functions based on external stimuli such as light or pH change, will enable more complex applications. One particular interesting application is the design of functional dye that can discriminate between live and dead cells or microorganisms [84–86]. Efforts to minimize cytotoxicity, enhance cellular uptake, and make these dyes more accessible through cost-effective and scalable synthesis are also vital for their broader adoption in clinical and research applications. These ongoing advancements ensure styryl-cyanine dyes will continue to play a crucial role in bioimaging, offering profound insights into biological processes and enabling more effective diagnostic and therapeutic strategies.

Appendix A. Supplementary data

Supplementary data associated with this article can be found at <https://dx.doi.org/10.2306/scienceasia1513-1874.2025.s008>. Additional references for supplementary tables are provided in references [87–101].

Acknowledgements: The authors acknowledge financial support from Ratchadapisek Somphot Fund for Postdoctoral Fellowship, Chulalongkorn University (to K.S.).

REFERENCES

- Gopika GS, Prasad PMH, Lekshmi AG, Lekshmypriya S, Sreesaila S, Arunima C, Kumar MS, Anil A, et al (2021) Chemistry of cyanine dyes: A review. *Mater Today Proc* **46**, 3102–3108.
- Deligeorgiev T, Vasilev A, Kaloyanova S, Vaquero JJ (2010) Styryl dyes – synthesis and applications during the last 15 years. *Color Technol* **126**, 55–80.
- Lincoln LL, Brooker LGS (1966) *United States Patent No. US3397981A*. United States Patent Office R., Eastman Kodak Company, NY.
- Zhao CF, Gvishi R, Narang U, Ruland G, Prasad PN (1996) Structures, spectra, and lasing properties of new (aminostyryl) pyridinium laser dyes. *J Phys Chem* **100**, 4526–4532.
- Dentani T, Nagasaka K-i, Funabiki K, Jin J-Y, Yoshida T, Minoura H, Matsui M (2008) Flexible zinc oxide solar cells sensitized by styryl dyes. *Dyes Pigm* **77**, 59–69.
- Lee C-C, Hu AT (2003) Synthesis and optical recording properties of some novel styryl dyes for DVD-R. *Dyes Pigm* **59**, 63–69.
- Huang JY, Lewis A, Loew L (1988) Nonlinear optical properties of potential sensitive styryl dyes. *Biophys J* **53**, 665–670.
- Krieg R, Eitner A, Halbhuber K-J (2011) Tailoring and histochemical application of fluorescent homo-dimeric styryl dyes using frozen sections: from peroxidase substrates to new cytochemical probes for mast cells, keratin, cartilage and nucleic acids. *Acta Histochem* **113**, 682–702.
- Tripathy M, Subuddhi U, Patel S (2020) A styrylpyridinium dye as chromogenic and fluorogenic dual mode chemosensor for selective detection of mercuric ion: application in bacterial cell imaging and molecular logic gate. *Dyes Pigm* **174**, 108054.
- Doyuran B, Gökoğlu E, Zouitini A, Keleş E, Taskin-Tok T, Seferoğlu N, Seferoğlu Z (2022) A novel fluorescent probe for the detection of cyanide ions in solutions and studies on its biophysical interactions with ctDNA and proteases. *J Fluoresc* **32**, 2173–2188.
- Noikham M, Sriwiphasathit C, Siriwong K, Vilaivan T (2023) Solvatochromic fluorescent styryl pyrene probes for the quantitative determination of water content in organic solvents. *Dyes Pigm* **208**, 110847.
- Saha S, Tiwari R, Parameswaran P, Patidar R, Srivastava N, Ranjan N (2025) Fluorescence based metabisulfite sensing: new aspects of ion sensing by a styryl benzothiazolium dye and understanding nitrite interference. *Spectrochim Acta A Mol Biomol Spectrosc* **324**, 124821.
- Zhang P, Fu C, Zhang Q, Li S, Ding C (2019) Ratiometric fluorescent strategy for localizing alkaline phosphatase activity in mitochondria based on the ES IPT process. *Anal Chem* **91**, 12377–12383.
- Yang Q, Wang S, Li D, Yuan J, Xu J, Shao S (2020) A mitochondria-targeting nitroreductase fluorescent probe with large Stokes shift and long-wavelength emission for imaging hypoxic status in tumor cells. *Anal Chim Acta* **1103**, 202–211.
- Kovalska VB, Kryvorotenko DV, Balanda AO, Losytskyy MY, Tokar VP, Yarmoluk SM (2005) Fluorescent homodimer styrylcyanines: synthesis and spectral-luminescent studies in nucleic acids and protein complexes. *Dyes Pigm* **67**, 47–54.

16. Mishra A, Behera RK, Behera PK, Mishra BK, Behera GB (2000) Cyanines during the 1990s: A review. *Chem Rev* **100**, 1973–2012.
17. Seferoğlu Z (2017) Recent synthetic methods for the preparation of charged and uncharged styryl-based NLO chromophores: A review. *Org Prep Proced Int* **49**, 293–337.
18. Mishra A, Behera RK, Mishra BK, Behera GB (1999) Dye-surfactant interaction: chain folding during solubilization of styryl pyridinium dyes in sodium dodecyl sulfate aggregates. *J Photochem Photobiol A Chem* **121**, 63–73.
19. Ribeiro Morais G, Vicente Miranda H, Santos IC, Santos I, Outeiro TE, Paulo A (2011) Synthesis and *in vitro* evaluation of fluorinated styryl benzazoles as amyloid-probes. *Bioorg Med Chem* **19**, 7698–7710.
20. Jaung J-y, Matsuoka M, Fukunishi K (1997) Syntheses and characterization of new styryl fluorescent dyes from DAMN. Part II. *Dyes Pigm* **34**, 255–266.
21. Felder S, Sagné C, Benedetti E, Micouin L (2022) Small-molecule 3D ligand for RNA recognition: tuning selectivity through scaffold hopping. *ACS Chem Biol* **17**, 3069–3076.
22. Gordo J, Avó J, Parola AJ, Lima JC, Pereira A, Branco PS (2011) Convenient synthesis of 3-vinyl and 3-styryl coumarins. *Org Lett* **13**, 5112–5115.
23. Cañeque T, Cuadro AM, Alvarez-Builla J, Pérez-Moreno J, Clays K, Castaño O, Andrés JL, Vaquero JJ (2014) Novel charged NLO chromophores based on quinoxilinium acceptor units. *Dyes Pigm* **101**, 116–121.
24. Faikhruea K, Supabowornsathit K, Angsujinda K, Aonbangkhen C, Chaikeeratisak V, Palaga T, Assavalapsakul W, Wagenknecht H-A, et al (2024) Nucleic acid-templated synthesis of cationic styryl dyes *in vitro* and in living cells. *Chem Eur J* **30**, e202400913.
25. Przhonska OV, Webster S, Padilha LA, Hu H, Kachkovski AD, Hagan DJ, VanStryland EW (2010) Two-photon absorption in near-IR conjugated molecules: design strategy and structure-property relations. In: Demchenko AP (ed) *Advanced Fluorescence Reporters in Chemistry and Biology I: Fundamentals and Molecular Design*, Springer Berlin Heidelberg, Berlin, Heidelberg, pp 105–147.
26. Haidekker MA, Nipper M, Mustafic A, Lichlyter D, Dakanali M, Theodorakis EA (2010) Dyes with segmental mobility: molecular rotors. In: Demchenko AP (ed) *Advanced Fluorescence Reporters in Chemistry and Biology I: Fundamentals and Molecular Design*, Springer Berlin Heidelberg, Berlin, Heidelberg, pp 267–308.
27. Kumbhar HS, Deshpande SS, Shankarling GS (2016) Aggregation induced emission (AIE) active carbazole styryl fluorescent molecular rotor as viscosity sensor. *ChemistrySelect* **1**, 2058–2064.
28. Singh A, Chaudhary D, Waghchoure AP, Kalariya RN, Bhosale RS (2021) Chapter eight: AIE materials for nucleus imaging. In: Bhosale RS, Singh V (eds) *Progress in Molecular Biology and Translational Science*, vol 184, Academic Press, pp 205–218.
29. Li Y, Huang Y, Sun X, Zhong K, Tang L (2023) An AIE mechanism-based fluorescent probe for relay recognition of HSO₃⁻/H₂O₂ and its application in food detection and bioimaging. *Talanta* **258**, 124412.
30. Yarmoluk SM, Kovalska VB, Volkova KD (2011) Optimized dyes for protein and nucleic acid detection. In: Demchenko AP (ed) *Advanced Fluorescence Reporters in Chemistry and Biology III: Applications in Sensing and Imaging*, Springer Berlin Heidelberg, Berlin, Heidelberg, pp 161–199.
31. Kumar CV, Turner RS, Asuncion EH (1993) Groove binding of a styrylcyanine dye to the DNA double helix: the salt effect. *J Photochem Photobiol A Chem* **74**, 231–238.
32. Supabowornsathit K, Faikhruea K, Ditmangklo B, Jaroenchuensiri T, Wongsuwan S, Junpra-ob S, Choopara I, Palaga T, et al (2022) Dicationic styryl dyes for colorimetric and fluorescent detection of nucleic acids. *Sci Rep* **12**, 14250.
33. Liu Q, Liu C, Chang L, He S, Lu Y, Zeng X (2014) Tunable PET process by the intercalation of cationic styryl dye in DNA base pairs and its application as turn-on fluorescent sensor for Ag⁺. *RSC Adv* **4**, 14361–14364.
34. Ustimova MA, Fedorov YV, Tsvetkov VB, Tokarev SD, Shepel NA, Fedorova OA (2021) Helical aggregates of bis(styryl) dyes formed by DNA templating. *J Photochem Photobiol A Chem* **418**, 113378.
35. Goshisht MK, Tripathi N, Patra GK, Chaskar M (2023) Organelle-targeting ratiometric fluorescent probes: design principles, detection mechanisms, bio-applications, and challenges. *Chem Sci* **14**, 5842–5871.
36. Ding Q, Luo Y, Hu J, Zhang S, Zhang W, Feng Y, Qian K, Li X, et al (2024) Recent progress on the organelle targeted AIEgens for bioimaging and treatment of diseases. *Chem Eng J* **495**, 153395.
37. Abeywickrama CS, Baumann HJ, Pang Y (2021) Simultaneous visualization of mitochondria and lysosome by a single cyanine dye: the impact of the donor group (-NR₂) towards organelle selectivity. *J Fluoresc* **31**, 1227–1234.
38. Hu L, Cao W, Jiang Y, Cai W, Lou X, Liu T (2024) Designing artificial fluorescent proteins and biosensors by genetically encoding molecular rotor-based amino acids. *Nat Chem* **16**, 1960–1971.
39. Wang K-N, Chao X-J, Liu B, Zhou D-J, He L, Zheng X-H, Cao Q, Tan C-P, et al (2018) Red fluorescent probes for real-time imaging of the cell cycle by dynamic monitoring of the nucleolus and chromosome. *Chem Commun* **54**, 2635–2638.
40. Wangngae S, Ngivprom U, Khrootkaew T, Worakaensai S, Lai R-Y, Kamkaew A (2023) Cationic styryl dyes for DNA labelling and selectivity toward cancer cells and Gram-negative bacteria. *RSC Adv* **13**, 2115–2120.
41. Srimongkol G, Ditmangklo B, Choopara I, Thanayavarn J, Dean D, Kokpol S, Vilaivan T, Somboonna N (2020) Rapid colorimetric loop-mediated isothermal amplification for hypersensitive point-of-care *Staphylococcus aureus* enterotoxin A gene detection in milk and pork products. *Sci Rep* **10**, 7768.
42. Gebhard J, Hirsch L, Schweddeheimer C, Wagenknecht H-A (2022) Hybridization-sensitive fluorescent probes for DNA and RNA by a modular “click” approach. *Bioconjugate Chem* **33**, 1634–1642.
43. Ditmangklo B, Taechalertpaisarn J, Siri Wong K, Vilaivan T (2019) Clickable styryl dyes for fluorescence labeling of pyrrolidinyl PNA probes for the detection of base mutations in DNA. *Org Biomol Chem* **17**, 9712–9725.
44. Zonjić I, Radić Stojković M, Crnolatac I, Tomašić Paić A, Pšeničnik S, Vasilev A, Kandinska M, Mondeshki M, et al (2022) Styryl dyes with *N*-methylpiperazine and *N*-phenylpiperazine functionality: AT-DNA and G-quadruplex binding ligands and theranostic agents.

- Bioorg Chem* **127**, 105999.
45. Patidar RK, Tiwari K, Tiwari R, Ranjan N (2023) Promoter G-quadruplex binding styryl benzothiazolium derivative for applications in ligand affinity ranking and as ethidium bromide substitute in gel staining. *ACS Appl Bio Mater* **6**, 2196–2210.
 46. Rhodes D, Lipps HJ (2015) G-quadruplexes and their regulatory roles in biology. *Nucleic Acids Res* **43**, 8627–8637.
 47. Masai H, Tanaka T (2020) G-quadruplex DNA and RNA: their roles in regulation of DNA replication and other biological functions. *Biochem Biophys Res Commun* **531**, 25–38.
 48. Chilka P, Desai N, Datta B (2019) Small molecule fluorescent probes for G-quadruplex visualization as potential cancer theranostic agents. *Molecules* **24**, 752.
 49. Yu Q-Q, Wang M-Q (2020) Carbazole-based fluorescent probes for G-quadruplex DNA targeting with superior selectivity and low cytotoxicity. *Bioorg Med Chem* **28**, 115641.
 50. Zheng B-X, Long W, Zhang Y-H, Huang X-H, Chen C-C, Zhong D-X, She M-T, Chen Z-X, et al (2020) Rational design of red fluorescent and selective G-quadruplex DNA sensing probes: the study of interaction signaling and the molecular structural relationship achieving high specificity. *Sens Actuators B Chem* **314**, 128075.
 51. Kang Y, Wei C (2022) Highly selective turn-on red fluorescence probes for visualization of the G-quadruplexes DNA in living cells. *Spectrochim Acta A Mol Biomol Spectrosc* **267**, 120518.
 52. Jiang C, Li S, Liu C, Liu R, Qu J (2023) A near-infrared cationic fluorescent probe based on thieno[3,2-*b*]thiophene for RNA imaging and long-term cellular tracing. *Sens Actuators B Chem* **378**, 133102.
 53. Fang L, Shao W, Zeng S-T, Tang G-X, Yan J-T, Chen S-B, Huang Z-S, Tan J-H, et al (2022) Development of a highly selective and sensitive fluorescent probe for imaging RNA dynamics in live cells. *Molecules* **27**, 6927.
 54. Chen X-C, Chen S-B, Dai J, Yuan J-H, Ou T-M, Huang Z-S, Tan J-H (2018) Tracking the dynamic folding and unfolding of RNA G-quadruplexes in live cells. *Angew Chem Int Ed* **57**, 4702–4706.
 55. Jensen KHR, Rekling JC (2010) Development of a no-wash assay for mitochondrial membrane potential using the styryl dye DASPEI. *SLAS Discov* **15**, 1071–1081.
 56. Ramadass R, Bereiter-Hahn J (2008) How DASPMI reveals mitochondrial membrane potential: fluorescence decay kinetics and steady-state anisotropy in living cells. *Biophys J* **95**, 4068–4076.
 57. Chevalier A, Zhang Y, Khdour OM, Kaye JB, Hecht SM (2016) Mitochondrial nitroreductase activity enables selective imaging and therapeutic targeting. *J Am Chem Soc* **138**, 12009–12012.
 58. Safir Filho M, Dao P, Martin AR, Benhida R (2020) Nitroreductase sensitive styryl-benzothiazole profluorescent probes for the visualization of mitochondria under normoxic conditions. *J Photochem Photobiol A Chem* **396**, 112528.
 59. She M-T, Yang J-W, Zheng B-X, Long W, Huang X-H, Luo J-R, Chen Z-X, Liu A-L, et al (2022) Design mitochondria-specific fluorescent turn-on probes targeting G-quadruplexes for live cell imaging and mitophagy monitoring study. *Chem Eng J* **446**, 136947.
 60. Mukherjee T, Aravintha Siva M, Bajaj K, Soppina V, Kanvah S (2020) Imaging mitochondria and plasma membrane in live cells using solvatochromic styrylpyridines. *J Photochem Photobiol B Biol* **203**, 111732.
 61. Efimova AS, Ustimova MA, Chmelyuk NS, Abakumov MA, Fedorov YV, Fedorova OA (2023) Specific fluorescent probes for imaging DNA in cell-free solution and in mitochondria in living cells. *Biosensors* **13**, 734.
 62. Zhang B-y, Wang P, Shi L, Ma X-y, Xi J-k, Zhang X-f (2023) A pH-sensitive fluorescent probe based on hemicyanine dyes for responding microenvironment changes of cardiomyocytes induced by Zn²⁺. *Microchem J* **193**, 109085.
 63. Xia T, Xia Z, Tang P, Fan J, Peng X (2024) Light-driven mitochondrion-to-nucleus DNA cascade fluorescence imaging and enhanced cancer cell photoablation. *J Am Chem Soc* **146**, 12941–12949.
 64. Betz WJ, Mao F, Bewick GS (1992) Activity-dependent fluorescent staining and destaining of living vertebrate motor nerve terminals. *J Neurosci* **12**, 363.
 65. Amaral E, Guatimosim S, Guatimosim C (2011) Using the fluorescent styryl dye FM1-43 to visualize synaptic vesicles exocytosis and endocytosis in motor nerve terminals. In: Chiarini-Garcia H, Melo RCN (eds) *Light Microscopy: Methods and Protocols*, Humana Press, Totowa, NJ, pp 137–148.
 66. Collot M, Boutant E, Fam KT, Danglot L, Klymchenko AS (2020) Molecular tuning of styryl dyes leads to versatile and efficient plasma membrane probes for cell and tissue imaging. *Bioconjugate Chem* **31**, 875–883.
 67. Abeywickrama CS, Wijesinghe KJ, Stahelin RV, Pang Y (2019) Red-emitting pyrene-benzothiazolium: unexpected selectivity to lysosomes for real-time cell imaging without alkalizing effect. *Chem Commun* **55**, 3469–3472.
 68. Pan Z, Wang Y, Chen N, Cao G, Zeng Y, Dong J, Liu M, Ye Z, et al (2023) Aggregation-induced emission photosensitizer with lysosomal response for photodynamic therapy against cancer. *Bioorg Chem* **132**, 106349.
 69. Liu C, Zhao T, He S, Zhao L, Zeng X (2020) A lysosome-targeting viscosity-sensitive fluorescent probe based on a novel functionalised near-infrared xanthene-indolium dye and its application in living cells. *J Mater Chem B* **8**, 8838–8844.
 70. Čipor I, Kurutos A, Dobrikov GM, Kamounah FS, Majhen D, Nestić D, Piantanida I (2022) Structure-dependent mitochondria or lysosome-targeting styryl fluorophores bearing remarkable Stokes shift. *Dyes Pigment* **206**, 110626.
 71. Protter DSW, Parker R (2016) Principles and properties of stress granules. *Trends Cell Biol* **26**, 668–679.
 72. Van Treeck B, Parker R (2019) Principles of stress granules revealed by imaging approaches. *Cold Spring Harbor Perspect Biol* **11**, a033068.
 73. Shao W, Zeng S-T, Yu Z-Y, Tang G-X, Chen S-B, Huang Z-S, Chen X-C, Tan J-H (2021) Tracking stress granule dynamics in live cells and *in vivo* with a small molecule. *Anal Chem* **93**, 16297–16301.
 74. Shao W, Wang J, Zeng S-T, Li Z-C, Chen S-B, Huang Z-S, Chen X-C, Tan J-H (2023) Development of a fluorescent chemical probe with the ability to visualize nascent phase-separated stress granules. *Sens Actuators B Chem* **394**, 134453.
 75. Groenning M (2010) Binding mode of Thioflavin T and

- other molecular probes in the context of amyloid fibril-current status. *J Chem Biol* **3**, 1–18.
76. Fiock KL, Betters RK, Hefti MM (2023) Thioflavin S staining and amyloid formation are unique to mixed tauopathies. *J Histochem Cytochem* **71**, 73–86.
 77. Gao G-Q, Xu A-W (2013) A new fluorescent probe for monitoring amyloid fibrillation with high sensitivity and reliability. *RSC Adv* **3**, 21092–21098.
 78. Li Q, Lee J-S, Ha C, Park CB, Yang G, Gan WB, Chang Y-T (2004) Solid-phase synthesis of styryl dyes and their application as amyloid sensors. *Angew Chem Int Ed* **43**, 6331–6335.
 79. Sulatskaya AI, Sulatsky MI, Povarova OI, Rodina NP, Kuznetsova IM, Lugovskii AA, Voropay ES, Lavysch AV, et al (2018) Trans-2-[4-(dimethylamino)styryl]-3-ethyl-1,3-benzothiazolium perchlorate – new fluorescent dye for testing of amyloid fibrils and study of their structure. *Dyes Pigm* **157**, 385–395.
 80. Gaur P, Galkin M, Kurochka A, Ghosh S, Yushchenko DA, Shvadchak VV (2021) Fluorescent probe for selective imaging of α -synuclein fibrils in living cells. *ACS Chem Neurosci* **12**, 1293–1298.
 81. Chernii S, Moshynets O, Aristova D, Kryvorotenko D, Losytskyy M, Iungin O, Yarmoluk S, Volynets G (2021) Benzoxazole styrylcyanine dye as a fluorescent probe for functional amyloid visualization in *Staphylococcus aureus* ATCC25923 biofilm. *Biopolym Cell* **37**, 447–458.
 82. Malleh R, Khan J, Pradhan K, Roy R, Jana NR, Jaisankar P, Ghosh S (2022) Design and development of benzothiazole-based fluorescent probes for selective detection of A β aggregates in Alzheimer's disease. *ACS Chem Neurosci* **13**, 2503–2516.
 83. Sangsuwan W, Faikhrua K, Supabowornsathit K, Sangsopon D, Ingrungruanglert P, Chuntakaruk H, Nuntavanotayan N, Nakprasit K, et al (2024) Design, synthesis, and characterization of novel styryl dyes as fluorescent probes for tau aggregate detection in vitro and in cells. *Chem Asian J* **19**, e202301081.
 84. Saint-Ruf C, Cordier C, M \acute{e} gret J, Matic I (2010) Reliable detection of dead microbial cells by using fluorescent hydrazides. *Appl Environ Microbiol* **76**, 1674–1678.
 85. Lee S, Bae S (2018) Evaluating the newly developed dye, DyeTox13 Green C-2 Azide, and comparing it with existing EMA and PMA for the differentiation of viable and nonviable bacteria. *J Microbiol Methods* **148**, 33–39.
 86. Niyomdechana N, Noisumdaeng P, Boonarkart C, Auewarakul P (2024) Effect of azo dye treatment on the detection of human (OC43) coronavirus surrogate and SARS-CoV-2 viability based on an in-house photoactivator device. *ScienceAsia* **50**, 2024077.
 87. Murphy MP, Smith RAJ (2007) Targeting antioxidants to mitochondria by conjugation to lipophilic cations. *Annu Rev Pharmacol Toxicol* **47**, 629–656.
 88. Cheng X, Feng D, Lv J, Cui X, Wang Y, Wang Q, Zhang L (2023) Application prospects of triphenylphosphine-based mitochondria-targeted cancer therapy. *Cancers* **15**, 666.
 89. Wu M-Y, Li K, Liu Y-H, Yu K-K, Xie Y-M, Zhou X-D, Yu X-Q (2015) Mitochondria-targeted ratiometric fluorescent probe for real time monitoring of pH in living cells. *Biomaterials* **53**, 669–678.
 90. Crawford H, Dimitriadi M, Bassin J, Cook MT, Abelha TF, Calvo-Castro J (2022) Mitochondrial targeting and imaging with small organic conjugated fluorophores: A review. *Chem Eur J* **28**, e202202366.
 91. Neikirk K, Marshall AG, Kula B, Smith N, LeBlanc S, Hinton A (2023) MitoTracker: A useful tool in need of better alternatives. *Eur J Cell Biol* **102**, 151371.
 92. Weiss MJ, Wong JR, Ha CS, Bleday R, Salem RR, Steele GD, Chen LB (1987) Dequalinium, a topical antimicrobial agent, displays anticarcinoma activity based on selective mitochondrial accumulation. *Proc Natl Acad Sci* **84**, 5444–5448.
 93. Zhitomirsky B, Farber H, Assaraf YG (2018) LysoTracker and MitoTracker Red are transport substrates of P-glycoprotein: implications for anticancer drug design evading multidrug resistance. *J Cell Mol Med* **22**, 2131–2141.
 94. Duan X, Tong Q, Fu C, Chen L (2023) Lysosome-targeted fluorescent probes: design mechanism and biological applications. *Bioorg Chem* **140**, 106832.
 95. Liu Q, Li J, Liu C, He S, Zhao L, Zeng X, Wang T (2021) Developing a NIR emitting benzothiazolium-thioxanthene dye and its application for the design of lysosomes-targeting palladium(II) probe. *Dyes Pigm* **196**, 109796.
 96. Kaya B, Smith H, Chen Y, Azad MG, Russell T, Richardson V, Bernhardt PV, Dharmasivam M, et al (2024) Targeting lysosomes by design: novel N-acridine thiosemicarbazones that enable direct detection of intracellular drug localization and overcome P-glycoprotein (Pgp)-mediated resistance. *Chem Sci* **15**, 15109–15124.
 97. Lin J, Yang K, New EJ (2021) Strategies for organelle targeting of fluorescent probes. *Org Biomol Chem* **19**, 9339–9357.
 98. Li D, Tian X, Wang A, Guan L, Zheng J, Li F, Li S, Zhou H, et al (2016) Nucleic acid-selective light-up fluorescent biosensors for ratiometric two-photon imaging of the viscosity of live cells and tissues. *Chem Sci* **7**, 2257–2263.
 99. Choi N-E, Lee J-Y, Park E-C, Lee J-H, Lee J (2021) Recent advances in organelle-targeted fluorescent probes. *Molecules* **26**, 217.
 100. Fischer RT, Stephenson FA, Shafiee A, Schroeder F (1984) Δ 5,7,9(11)-cholestatrien-3 β -ol: a fluorescent cholesterol analogue. *Chem Phys Lipids* **36**, 1–14.
 101. Zwicker VE, Oliveira BL, Yeo JH, Fraser ST, Bernardes GJL, New EJ, Jolliffe KA (2019) A fluorogenic probe for cell surface phosphatidylserine using an intramolecular indicator displacement sensing mechanism. *Angew Chem Int Ed* **58**, 3087–3091.

Appendix A. Supplementary data

Table S1 Common organelle-targeting groups that are employed for molecular design of organelle-specific dyes (adapted from Ref. [35] which was published under the Creative Commons Attribution License (CC BY)).

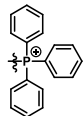
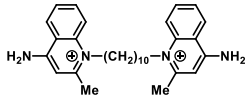
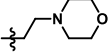
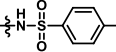
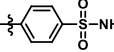
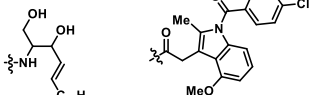
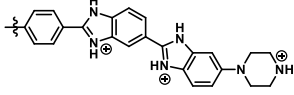
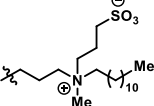
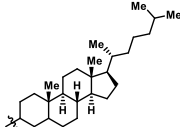
Organelle	Targeting groups	Ref.
Mitochondria		[87, 88]
		[89]
		[90]
		[91]
		[92]
Lysosome		[93]
		[94]
		[95]
		[96]
Endoplasmic reticulum		[97]
		
Golgi apparatus		[97]
		
Nucleus		[98]
		[97]
Cell membrane		[99]
		[100]
	$\text{C}_{17}\text{H}_{35}$	[101]

Table S2 Selected styryl-cyanine dyes for bioimaging of nucleic acids.

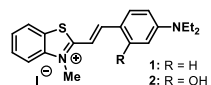
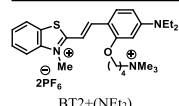
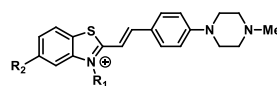
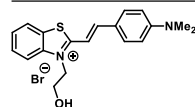
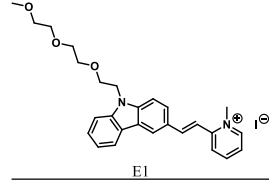
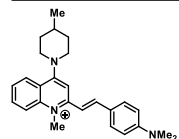
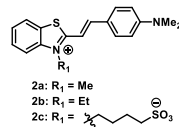
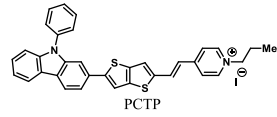
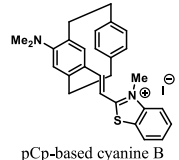
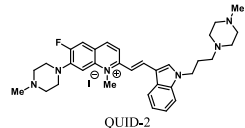
Structure	Wavelength of detection	Target	Remarks	Ref.
	$\lambda_{\text{ex}} = 543 \text{ nm}$ $\lambda_{\text{em}} = 600 \pm 20 \text{ nm}$	DNA/RNA	The dyes selectively image the nucleolus during interphase and the chromosomes during mitosis, demonstrating significant potential for real-time fluorescence monitoring of dynamic transitions from the nucleolus to chromosomes throughout the entire cell cycle.	[39]
	$\lambda_{\text{ex}} = 488 \text{ nm}$ $\lambda_{\text{em}} = 565 \text{ nm}$ (Styryl-QL) and 547 nm (Styryl-BT)	DNA	The dyes exhibit selectivity toward dsDNA, cancer cells, and Gram-negative bacteria (<i>S. aureus</i>), highlighting their dual functionality as bioimaging agents and therapeutic tools with both anti-cancer and antibacterial properties.	[40]
	$\lambda_{\text{ex}} = 565 \text{ nm}$ $\lambda_{\text{em}} = 600 \text{ nm}$	DNA/RNA	The dicationic dye displayed a higher binding affinity for nucleic acids compared to monocationic dye, with excellent sensitivity for dsDNA detection (LOD = 1.2 ng/ml or 0.07 nM in fluorescence mode).	[32, 41]
	$\lambda_{\text{ex}} = 442\text{--}476 \text{ nm}$ $\lambda_{\text{em}} = 572\text{--}585 \text{ nm}$	DNA/RNA	The dyes with <i>N</i> -methylpiperazine substituent exhibit a strong fluorescence enhancement with AT-rich DNA sequences, demonstrating binding to the minor groove.	[44]
	$\lambda_{\text{ex}} = 532 \text{ nm}$ $\lambda_{\text{em}} = 598 \text{ nm}$	G4 DNA (Pu22/c-Myc)	The dye exhibits selective binding to G-quadruplexes corresponding to promoter regions (Pu22/c-Myc), with a 1:1 binding stoichiometry and an association constant (K_a) of $1.12 \times 10^6 \text{ M}^{-1}$.	[45]
	$\lambda_{\text{ex}} = 400 \text{ nm}$ $\lambda_{\text{em}} = 545 \text{ nm}$	G4 DNA	The dye binds preferentially to G-quadruplex DNA over duplex DNA and other biomolecules via end-stacking. It can penetrate living cells, localizing primarily in the cytoplasm with low cytotoxicity.	[49]
	$\lambda_{\text{ex}} = 498 \text{ nm}$ $\lambda_{\text{em}} = 610 \text{ nm}$	G4 DNA	The dye exhibits high selectivity for the c-myc pu27 G-quadruplex structures with high binding affinity, making it and also demonstrated in live cell imaging.	[50]
	$\lambda_{\text{ex}} = 561 \text{ nm}$ $\lambda_{\text{em}} = 575\text{--}630 \text{ nm}$	G4 DNA	The dyes induce folding of bcl-2 DNA to form G-quadruplex structures. The dyes with <i>N</i> -methyl and <i>N</i> -ethyl side chains exhibit higher affinity for G-quadruplex DNA than the dye with sulfonate side chain.	[51]
	$\lambda_{\text{ex}} = 561 \text{ nm}$ $\lambda_{\text{em}} = 595\text{--}710 \text{ nm}$	RNA	The dye distinguishes RNA from DNA in solution and cells, showing 52.2-fold fluorescence increase upon RNA binding. It demonstrates low detection limit for RNA of 2.17 $\mu\text{g/ml}$, along with low cytotoxicity, good biocompatibility, and excellent photostability.	[52]
	$\lambda_{\text{ex}} = 550 \text{ nm}$ $\lambda_{\text{em}} = 640 \text{ nm}$	RNA	The paracyclophane-based 3D dye preferentially binds to RNA octaloops over smaller loop sizes. This structural modification also influences the dye's behavior in cells, highlighting the impact of shape design on RNA-binding specificity.	[21]
	$\lambda_{\text{ex}} = 470 \text{ nm}$ $\lambda_{\text{em}} = 555 \text{ nm}$	RNA	The dye shows excellent selectivity to RNA over DNA with low limit of detection (1.8 ng/ml in solution).	[53]

Table S3 Selected styryl-cyanine dyes for bioimaging of cellular organelles.

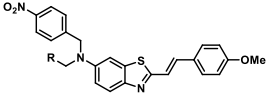
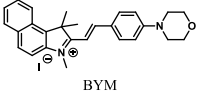
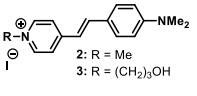
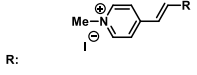
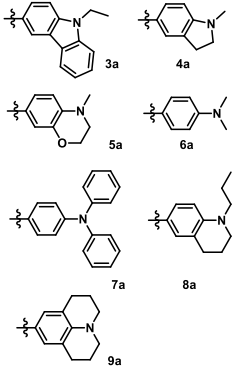
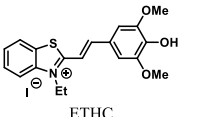
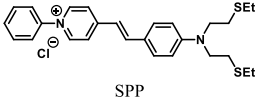
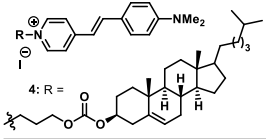
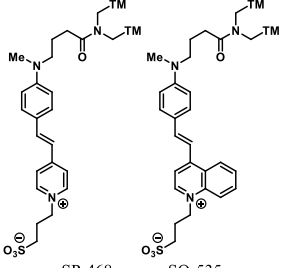
Structure	Wavelength of detection	Target	Remarks	Ref.
 <p>MitoP-2: R = Me MitoP-3: R = (CH₂)₂-PPh₃⁺T</p>	$\lambda_{\text{ex}} = 405 \text{ nm}$ $\lambda_{\text{em}} = 520 \text{ nm}$	Mitochondria	The dyes specifically stained the mitochondria, as confirmed by a co-localization experiment with MitoTracker Deep Red. The presence of the <i>p</i> -nitrobenzyl unit allows detection of mitochondrial NTR activity.	[58]
 <p>BYM</p>	$\lambda_{\text{ex}} = 530 \text{ nm}$ $\lambda_{\text{em}} = 615 \text{ nm}$	Mitochondria	The dye selectively targets mitochondria without entering the nucleus and exhibits high specificity for mitochondrial G-quadruplex DNA (G4-DNA).	[59]
 <p>2 and 3 2: R = Me 3: R = (CH₂)₂OH</p>	$\lambda_{\text{ex}} = 450 \text{ nm}$ $\lambda_{\text{em}} = 600 \text{ nm}$	Mitochondria	The dyes efficiently image and track mitochondria, as demonstrated by co-localization experiments with HeLa cells expressing FP-tagged mitochondria-specific markers, MitoDsRed and Mito-ECFP.	[60]
 <p>R:</p>  <p>3a, 4a, 5a, 6a, 7a, 8a, 9a</p>	$\lambda_{\text{ex}} = 488 \text{ nm}$ $\lambda_{\text{em}} = 595\text{--}650 \text{ nm}$	Mitochondria	All of the studied dyes are expected to exhibit specific localization within mitochondria, based on the calculated physicochemical parameters and the binding parameter to nucleic acids, LCF (largest conjugated fragment; proportional to the area of the coplanar aromatic region).	[61]
 <p>ETHC</p>	$\lambda_{\text{ex}} = 405 \text{ nm}$ (neutral form) 559 nm (deprotonated form) $\lambda_{\text{em}} = 547 \text{ nm}$ (neutral form) 603 nm (deprotonated form)	Mitochondria, Nucleus	This pH sensitive dye exhibits two different emission bands which enables dual-channel imaging of both the nucleus and mitochondria. The pH sensitivity also allows for monitoring pH changes in mitochondria.	[62]
 <p>SPP</p>	$\lambda_{\text{ex}} = 486\text{--}488 \text{ nm}$ $\lambda_{\text{em}} = 600\text{--}650 \text{ nm}$	Mitochondria, Nucleus	The dye migrates from mitochondria to the nucleus in the presence of light. This unique property allows the dye to track nucleic acid damage in both mitochondria and nuclei, providing insights into critical cellular processes such as apoptosis.	[63]
 <p>4: R =</p>	$\lambda_{\text{ex}} = 450 \text{ nm}$ $\lambda_{\text{em}} = 600 \text{ nm}$	Cell membrane	The cholesterol-tethered styrylpyridine dye efficiently stains the plasma membrane and shows strong co-localization with the plasma membrane labeled by ECFP-MEM.	[60]
 <p>SP-468, SQ-535</p>	$\lambda_{\text{ex}} = 468 \text{ nm}$ (SP-468), 535 nm (SQ-535) $\lambda_{\text{em}} = 600 \text{ nm}$ (SP-468), 665 nm (SQ-535)	Cell membrane	The dyes were developed as cellular membrane probes, exhibiting a large Stokes shift and high photostability in both live and fixed cell and tissue samples.	[66]

Table S3 Continue

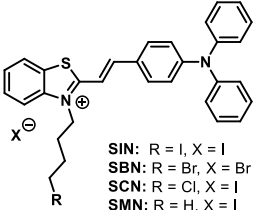
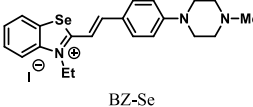
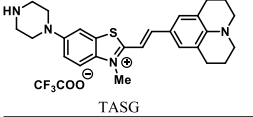
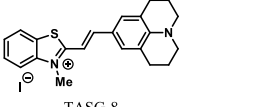
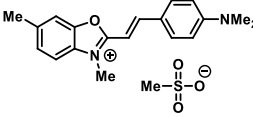
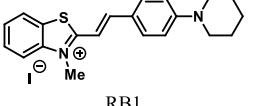
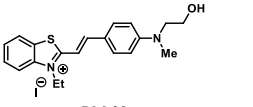
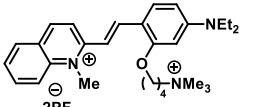
Structure	Wavelength of detection	Target	Remarks	Ref.
 <p>SIN: R = I, X = I SBN: R = Br, X = Br SCN: R = Cl, X = I SMN: R = H, X = I</p>	$\lambda_{\text{ex}} = 530 \text{ nm}$ $\lambda_{\text{em}} = 658\text{--}666 \text{ nm}$	Lysosome	The SIN dye exhibits high specificity for lysosomes, with a co-localization factor of 0.97 with LysoTracker in HeLa cells.	[68]
 <p>BZ-Se</p>	$\lambda_{\text{ex}} = 458 \text{ nm}$ $\lambda_{\text{em}} = 588 \text{ nm}$	Lysosome	The dye exhibits lysosome-specific localization, with a high co-localization factor with LysoTracker (Pearson correlation coefficient, $r = 0.837$).	[70]
 <p>TASG</p>	$\lambda_{\text{ex}} = 560 \text{ nm}$ $\lambda_{\text{em}} = 625\text{--}650 \text{ nm}$	Aggregated nucleoprotein (stress granules)	The dye can detect SG in fixed and live cells, <i>ex vivo</i> and <i>in vivo</i> , and reveal SG dynamics in living cells and organisms.	[73]
 <p>TASG-8</p>	$\lambda_{\text{ex}} = 560 \text{ nm}$ $\lambda_{\text{em}} = 613 \text{ nm}$	Aggregated nucleoprotein (stress granules)	The dye offers several advantages over the original dye (TASG), including the ability to effectively label small nascent SGs in both fixed and living cells.	[74]

Table S4 Selected styryl-cyanine dyes for bioimaging of protein aggregates.

Structure	Wavelength of detection	Target	Remarks	Ref.
	$\lambda_{\text{ex}} = 532 \text{ nm}$ $\lambda_{\text{em}} = 579 \text{ nm}$	Amyloid fibrils	The dye exhibits a selective response to β -lactoglobulin amyloid fibrils amyloid fibrils, with a 214-fold fluorescence enhancement. This is significantly higher than other biomolecules, including DNA and RNA, and lysozyme amyloid fibrils.	[81]
 <p>RB1</p>	$\lambda_{\text{ex}} = 570 \text{ nm}$ $\lambda_{\text{em}} = 605 \text{ nm}$	α -Synuclein (α -Syn) amyloid fibrils	The dye exhibits a 76 nm red-shifting of absorption maxima and 112-fold fluorescence enhancement upon binding to amyloid fibrils ($K_d = 30 \text{ nM}$). This shift allows selective excitation of the dye in its bound form.	[80]
 <p>RM-28</p>	$\lambda_{\text{ex}} = 508 \text{ nm}$ $\lambda_{\text{em}} = 589 \text{ nm}$	Amyloid beta peptide ($A\beta$)	The dye exhibits high sensitivity (7.5-fold fluorescence enhancement) and high affinities toward $A\beta$ aggregates ($K_d = 175.69 \pm 4.8 \text{ nM}$).	[82]
 <p>2PF₆</p>	$\lambda_{\text{ex}} = 561 \text{ nm}$ $\lambda_{\text{em}} = 592 \text{ nm}$	Aggregated tau protein	The dye exhibits 28-fold fluorescence enhancement upon binding to tau aggregates <i>in vitro</i> , and demonstrated selective binding to tau aggregates in living cells.	[83]